Pergamon

Journal of Structural Geology, Vol. 16, No. 4, pp. 467 to 475, 1994

0191-8141/94 $6.00 + 0.00

0191-8141(93)E0006-7

The role of asymmetry in the formation of structures

DECLAN G. DE PAOR

Geology Department, George Washington University, Washington, DC 20052, U.S.A.

(*Received* 15 *January* 1993; *accepted in revised form* 27 *October* 1993)

Abstract—Asymmetric fabrics elements abound in deformed rocks. They are best understood by revising our assumptions regarding the symmetry, homogeneity and steadiness of the stress, strain and kinematic regimes operative during tectonism. With the aid of new off-axis Mohr circle constructions, the ramifications of asymmetric tensor phenomena may be evaluated and the link between theory and observation may be strengthened. Stress in rocks is always a symmetric tensor phenomenon under conditions of equilibrium and homogeneity but it may be asymmetric in certain circumstances, resulting in the development of only one of a possible pair of symmetric conjugate structures. Deformation is generally asymmetric and is often modeled as the outcome of steady flow, whereas it may be the cumulative result of unsteady, or accelerating, flow. Polar loci of normal and shear stresses, longitudinal and shear strains, and rotations illustrate effects which may help explain natural patterns of fabric asymmetry. This theoretical treatment provides the basis for evaluating field and laboratory observations that might otherwise to considered contradictory or polydeformational.

INTRODUCTION

IN AN attempt to better understand the fabrics of deformed rocks, structural geologists have extended theoretical analyses beyond basic models of pure shear and simple shear deformation. At the Penrose Conference whose proceedings are reported in this Special Issue, much discussion concerned the recognition of pure and simple components of general shear deformation in rocks. However, whilst the general shear model currently in vogue improves upon pure and simple shear end members, it is still highly restrictive. The pure shear component of deformation is assumed to act orthogonal to the plane of simple shear, the flow regime leading to deformation is generally assumed to be steady-state and the causal stress regime is assumed to be always in equilibrium and therefore symmetric. The purpose of this paper is to go beyond the limits of these simplifying assumptions and examine the implications of general non-equilibrium stress, general non-steady flow and accelerating shear deformation for the development of structures in rocks.

STRESS THEORY

The symmetry of stress

Textbooks and other standard references on stress in structural geology begin with a proof that stress is a symmetric tensor. Consider the surface forces $\mathbf{F}_1, \mathbf{F}_2, \mathbf{F}_3, \mathbf{F}_4, \ldots$ etc., acting on an elemental area. Let $\mathbf{F}_i$ be one surface force distributed across a *cross-sectional* area A and let $\mathbf{n}$ be a unit vector normal to a plane; $\mathbf{n}$ is inclined at an angle θ to the line of the force. The stress on the cross-sectional plane is $\mathbf{F}_i/A$ and the stress on the inclined plane of area A' is $F_i/(A/\cos\theta)$ or more simply

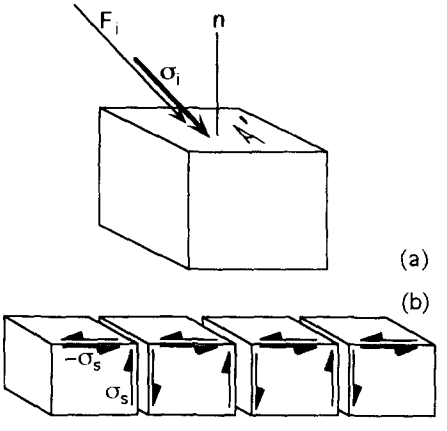

Fig. 1. (a) Classical construction for illustrating the stress σ_i on a cubic element face of area A' and unit normal $\mathbf{n}$ due to the action of a surface force $\mathbf{F}_i$. (b) σ_s is the dextral shear stress on the sides of the cubes; $-\sigma_s$ is the sinistral shear stress on the tops of the cubes (see text).

$$\sigma_i = \mathbf{F}_i * \mathbf{n}, \tag{1}$$

where $A = 1$, σ_i denotes the stress contributed by the i-th force and the star product $\mathbf{F}_i * \mathbf{n}$ (De Paor 1990) denotes a vector in the direction of the force $\mathbf{F}_i$ with magnitude equal to the dot product $\mathbf{F}_i \cdot \mathbf{n}$ (Fig. 1a). The total stress σ_t resulting from all surface forces $i = 1, 2, 3, 4 \ldots$, acting on the plane is given by

$$\sigma_t = \sum_i (\mathbf{F}_i * \mathbf{n}). \tag{2}$$

As $\mathbf{n}$ varies in trend and plunge, the total stress σ_t describes an ellipsoid—the stress ellipsoid (some textbooks complicate matters by the mistakenly summing the forces first—$\Sigma_i(\mathbf{F}_i) * \mathbf{n}$ gives a line, not an ellipsoid, and is not a correct expression of the stress state).

The total stress σ_t may be resolved into components of normal stress σ_n and shear stress σ_s acting, respectively, perpendicular and parallel to the plane,

$$\sigma_n = \mathbf{n} * \sigma_t \quad (3)$$

and

$$\sigma_s = \sigma_t - \sigma_n \quad (4)$$

(see De Paor 1990).

Now consider the plane to be one side of an elemental cube. According to the standard argument, in a homogeneous system at equilibrium, the magnitudes of normal and shear components of stress on opposite cube faces must be equal, for otherwise the cube might begin to travel in the direction of the resultant force and/or spin with the sense of the resultant couple. This proof explicitly excludes inhomogeneous force fields or conditions of disequilibrium. In the case of inhomogeneity, a gradient may exist in the shear stresses acting on the tops of neighboring cubic elements (Fig. 1b) and the requirement of symmetry (equal opposite shear stresses on tops and sides of cubes) places a severe restriction on how the stress field can vary in space. By analogy with strain, it is difficult to envisage heterogeneous deformation gradients in a field which is everywhere irrotational (difficult but not impossible: heterogeneous compaction in a sedimentary setting and flattening in the aureole of a perfectly spherical intrusion are two solutions). If a body is in disequilibrium, the forces acting on an element do not balance but are divisible into a balance of forces which deform the body, a resultant force which displaces it and a couple which rotates it.

Table 1. Notation

A	area of plane
a, b, c	arbitrary lines
d	dextral
$\mathbf{F}_i$	i-th surface force
F	Mohr envelope for pre-fractured rock
i	arbitrary integer
I	Mohr envelope for intact rock
$\mathbf{n}$	unit normal vector
p	pole to Mohr stress circle
P	pole to Mohr strain circle
q	second intersection point (stress)
Q	second intersection point (strain)
Q_a, Q_b, Q_c	second intersection points (arbitrary lines)
Q_0	second intersection point (initial state)
$Q^\perp$	second intersection point (perpendicular line)
s	sinistral
S	stretch (final/initial length)
S^-	stretch of perpendicular line
t	trace of plane
α	rotation (change in orientation)
α'	angular velocity
ε'	strain rate
ε''	acceleration
ϕ	angle of stability
ψ	angular shear
γ	shear strain
ν	angle between eigenvectors
$\Delta\nu$	change in ν
σ_i	stress due to surface force $\mathbf{F}_i$
σ_1, σ_2	principal stresses
σ	total stress on a plane
σ_n, σ_s	normal and shear stress components
σ'	total stress on perpendicular plane
σ'_n, σ'_s	normal and shear components of σ'
$\bar{\sigma}_s$	mean shear stress
σ_i	sum over i
$\cdot$	dot product
$*$	star product

Malvern (1969) presents a more general proof of stress symmetry based on Cauchy's equations of motion but nevertheless accepts the existence of asymmetric or 'couple stress' conditions when the force field is non-conservative. Indeed, asymmetric stress, or 'couple stress', has been extensively discussed in the classical mechanics literature (see Voigt 1887, 1895, Cosserat & Cosserat 1909, Huen 1913, Günter 1958, Kröner 1960 as reviewed in Truesdell & Toupin 1960; also see Biot 1965). In physics, couple stresses are known to occur in magnetic materials under a high magnetic field, for example. In the field of structural geology, De Paor (1981) pointed out some of the implications of stress asymmetry for rocks. A complete discussion of asymmetric stress theory is beyond the scope of this paper.

Koenemann (1992, and oral and personal communications) argues that classical mechanics, since the time of Cauchy, is fundamentally flawed and that stress is always asymmetric. It would be unfortunate if those who reject these arguments were to ignore the possibilities of stress asymmetry in special geological settings, for example in the vicinities of fault tips during short periods of crack initiation or propagation. This paper does not propose to prove the existence of such circumstances, but rather to investigate the possible ramifications for structures *if* stress is ever asymmetric in rocks.

The modified Mohr construction for stress

To clarify the relationship between orientations of planes and stresses acting upon them in two dimensions, Fig. 2(a) illustrates a symmetric stress state defined by principal stresses, σ_1 and σ_2, along with the stress acting on an arbitrary plane σ and its shear and normal components σ_s and σ_n, parallel to the plane's trace, t, and normal, n, respectively. The plane's trace is shaded to distinguish it from the normal and the angle of stability ϕ (the angle whose tangent is σ_s/σ_n), is also shown. The stress state is represented in Fig. 2(b) by a Mohr circle with pole p (see Allison 1984). The circle is centered on the horizontal normal stress axis which it intersects at σ_1 and σ_2. Lines joining these points to the pole define the principal directions. The vertical co-ordinate axis is shaded like a plane's trace so as to emphasize the fact that angles between stress vectors and this axis in Mohr space are equal to equivalent angles between stress vectors and planes in geographic space.

Following the classical construction (e.g. Mandl 1988, p. 239), the stress σ on a given plane, t, is obtained by drawing a parallel line through p and marking its intersection with the circle at σ (Fig. 2c). The main disadvantage of this construction is that it gives the incorrect sense for the shear stress, σ_s, and angle of stability, ϕ, relative to the normal and shear axes. It is essential to address this problem before introducing off-axis Mohr circles for asymmetric stress in order to avoid confusion. Figure 2(d) shows an alternative stress construction using the 'second kind' of Mohr circle (De Paor & Means 1984). To determine the stress on a plane of trace t, a shaded line is drawn through the pole, p, to meet the

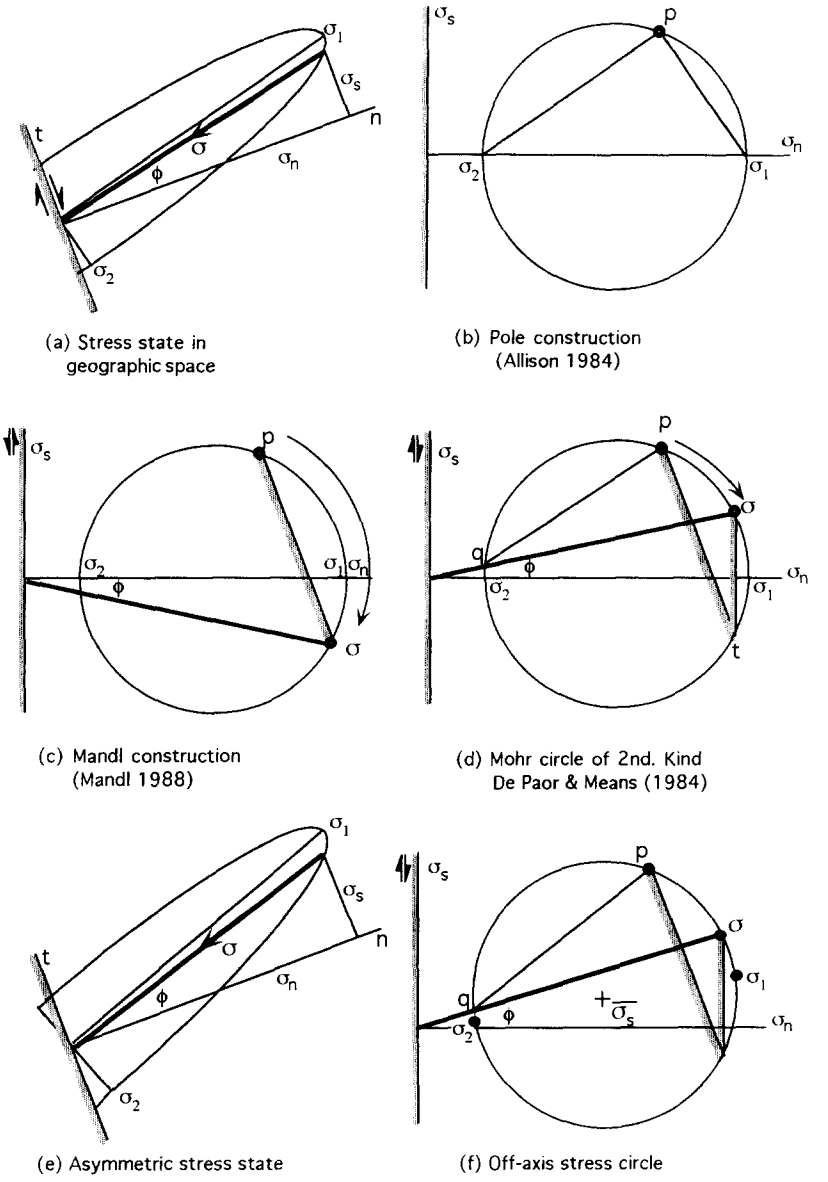

Fig. 2. (a) Stress, σ, on a plane trace, t (shaded), in a stress state defined by the ellipse with principal semiaxes σ_1 and σ_2. n is the normal to the plane, σ_n and σ_s are normal and shear stress components, and ϕ is the angle of stability. (b) Pole construction for the stress state in (a). P is the pole; lines joining it to σ_1 and σ_2 are parallel to the principal stresses (see Allison 1984). (c) Mandl's (1988) convention for the stress construction. Arrow indicates relation between pole p and stress σ on given plane (shaded). Note that the shear stress, σ_s, and angle of stability, ϕ, are reversed from (a). (d) De Paor & Means's (1984) convention for the stress construction (second kind). Arrow indicates relation between pole p and stress on plane σ. q is second point of intersection of stress σ with circle and pq is parallel to the direction of σ in geographic space. All angles are correct in sense when compared with (a). (e). Asymmetric stress: note enhanced dextral shear component, σ_s. (f) Off-axis construction for asymmetric stress. $\bar{\sigma}_s$ is the mean shear stress. Other symbols are in (d).

circle at t. Point p is then moved around the circle until the shaded line is vertical, parallel to the shaded σ_s axis. This gives the total stress, σ, with a correct sense of shear stress, σ_s, and also a correct sense for the stability angle, ϕ. In addition to resolving the reversal of shear sense problem, the construction has a new property (De Paor 1987); the direction of the stress vector, σ, in geographical space is parallel to p–q, where q is the second point of intersection of the stress, σ, with the Mohr circle.

The off-axis Mohr construction for stress

The case of asymmetric stress is illustrated in Figs. 2(e) & (f) where the plane, t, and its normal, n, are unchanged from Fig. 2(a). The stress circle and its pole, p, are shifted off-axis by an amount $\bar{\sigma}_s$, the mean shear stress. The maximum and minimum principal stresses are marginally greater in magnitude; they are represented on the Mohr circle by diametrically opposite points furthest from and nearest to the origin but, being off-axis, they are no longer directions of zero shear stress and they act on an orthogonal pair of planes to which they are slightly oblique. There are two directions of zero shear stress in the case illustrated in Fig. 2(f) because the Mohr circle intersects the horizontal, $\sigma_s = 0$, co-ordinate axis twice, but they are not orthogonal directions; they could be only one or none if $\bar{\sigma}_s$ equalled or exceeded the radius of the circle, as the points of intersection of the circle and the normal stress axis

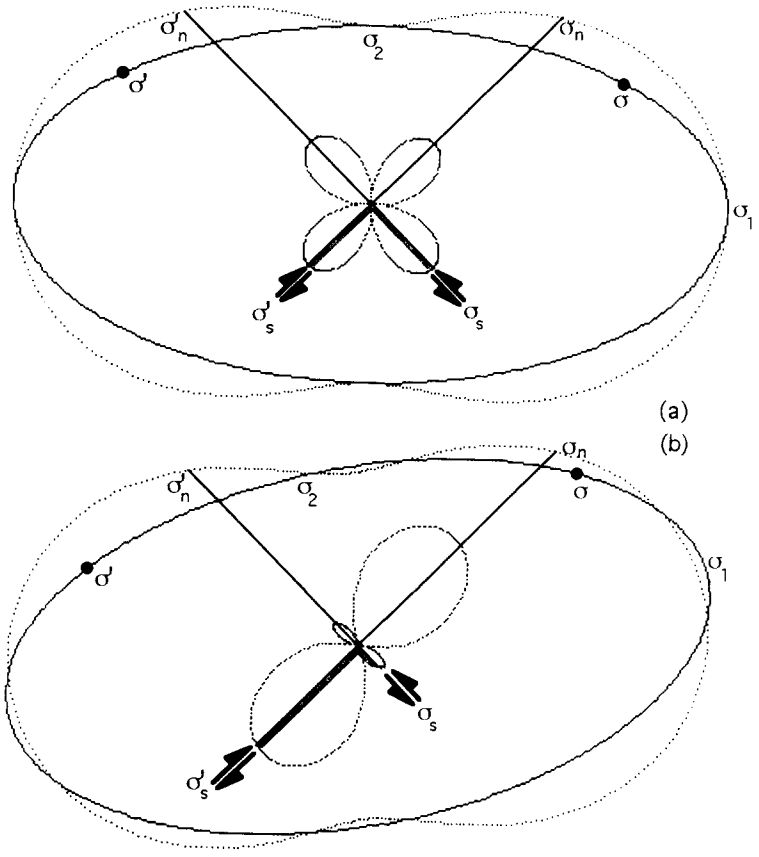

Fig. 3. Loci of normal (dotted) and shear (dashed) stresses drawn as polar graphs with origin at center of the stress ellipse. Two plane traces (shaded), one primed, the other unprimed are shown at ±45° to the horizontal; they intersect the shear stress locus at a distance equal to the shear stress acting on them. Normals intersect the σ_n locus at a distance equal to the normal stress on the plane. Total stress acting on each plane is indicated by dots. (a) Symmetric case: note the four-fold symmetry of the shear locus which means that shear stresses on orthogonal planes are equal in magnitude. (b) Asymmetric case: note asymmetric orientation and two-fold symmetry of both loci.

would then become complex numbers. The most important difference between the illustrated symmetric and asymmetric stress states is that dextral shear stresses are enhanced in the latter case. The curious, apparently sinistral, effect upon the orientation of the stress ellipse results from the conventional treatment of compressive stresses as positive in geological studies.

Figure 3 shows polar loci of normal and shear stress for (a) symmetric and (b) asymmetric stress states (reproduced from De Paor 1981). The principal stresses, σ_1 and σ_2, act on vertical and horizontal planes in both (a) and (b). A ray drawn outwards from the center of each plot represents the direction of the pole to a plane and the distance along the ray to the dotted locus represents the normal stress on the plane, σ_n. A shaded perpendicular line represents the trace of the plane and the distance out along it to the dashed locus indicates the shear stress, σ_s. The locus of total stress, σ, is the stress ellipse itself (solid line) and a dot marks the total stress vector for the plane in question. The primed quantities, σ'_n, σ'_s and σ', are the normal, shear and total stresses on a perpendicular plane. Normal stresses, σ_n and σ'_n, are equal in the symmetric case only because the primed and unprimed planes were chosen at ±45° to the principal directions: in the asymmetric case, normal stresses are marginally different. Shear stresses, σ_s and σ'_s, are equal in magnitude on any pair of perpendicular planes in the symmetric case (the shear stress locus has four-fold symmetry), but in the asymmetric case, shear stresses on perpendicular planes are clearly different. These loci have implications for regional stress analyses (e.g. Engelder & Geiser 1980) where stress asymmetries may result in very different populations of conjugate faults, for example.

Couple stress and Riedel shears

To investigate the consequences of couple stress further, Figs. 4(a) & (b) illustrate changes with depth of the Mohr envelope for stress in conjunction with a Mohr stress circle (cf. Bayly 1992, p. 201). The effective stress state is given by the position of each Mohr circle relative to the corresponding Mohr envelope (moving the envelope to the right instead of moving the circle to the left gives a much clearer indication of the actual stresses at failure). With increasing depth, pore pressure drives the envelope to the right and increasing total stresses drive the Mohr circle also to the right. The circle's radius is increased as a result of enhanced stress difference during tectonism. Depending on the relative magnitudes of these changes, effective stresses may increase or decrease. Passing down through an over-pressured zone,

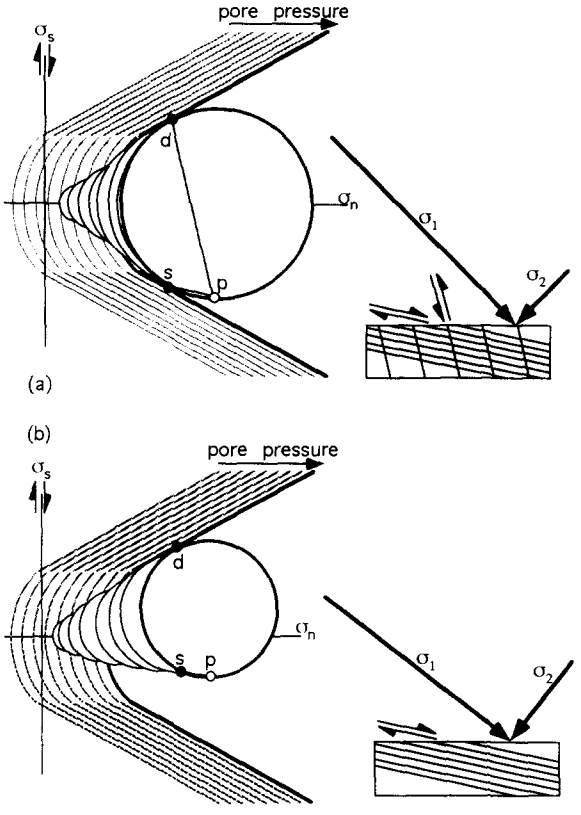

Fig. 4. Interpretation of Riedel shears using Mohr constructions (see text). (a) Symmetric case: the applied stress and pore pressure build up until Mohr envelope and circle touch at two points, leading to conjugate Riedel shear structures indicated by short arrow. d = dextral stress acting on plane parallel to sp; s = sinistral stress acting on plane parallel to dp. (b) Asymmetric stress build-up with development of only the dextral shear set from (a).

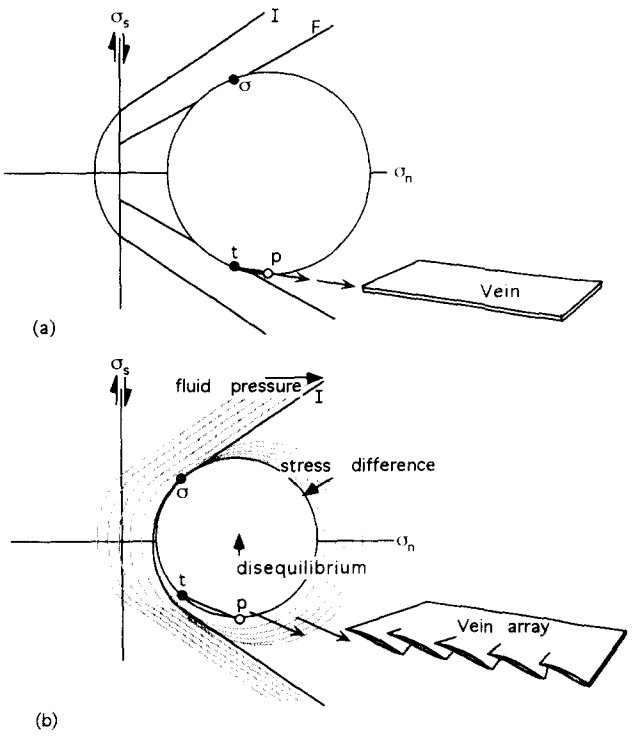

Fig. 5. (a) Fracturing along vein parallel to tp owing to stress σ which lies on the linear failure envelope F (any stress σ in the arc of the Mohr circle intersected by F is unstable for a pre-existing fracture). (b) Development of en échelon veins by a combination of stress difference, disequilibrium and fluid pressure. The vein orientation tp is steeper than in (a) because the point of tangency σ of the Mohr circle and intact rock envelope I is different. Note that stress asymmetry is required to prevent development of a conjugate vein orientation σ–p.

the envelope is displaced more rapidly than the circle and eventually touches it, signifying failure. In Fig. 4(a), the stress state is symmetric and there are two simultaneous failure planes developed. Their directions in space are obtained by the pole construction of Fig. 2(d) and correspond to classical Riedel shear directions. For a maximum principal stress oriented at 45° to a shear zone boundary the pole, p, is located at the lowest point on the circle. Dextral shear failure (stress = d) occurs on planes whose orientation is obtained by joining the opposite point (plane = s) to the pole, p. Similarly, sinistral shear failure (stress = s) occurs on planes whose orientation is obtained by joining the opposite point (plane = d) to the pole, p (see Fig. 2d).

In Fig. 4(b), by contrast, the stress state is asymmetric with enhanced dextral shear. Consequently, the Mohr circle touches the Mohr envelope at one point, d; the high-angle, sinistral, antithetic Riedel shear set does not develop in this case. The orientation of the dextral Riedel failure set (stress = d) is obtained again by joining the opposite point (plane = s), to the pole p (Fig. 4b). Figure 4(b) may exaggerate the degree of asymmetry which might occur in practice but it is important to note that an infinitesimal departure from symmetry in the stress may be sufficient to suppress the development of conjugate failure planes.

Couple stress and en échelon vein arrays

Stress asymmetry also has implications for the development of vein arrays. Figure 5 shows the failure envelope for a pre-existing fracture plane F which is weaker than the envelope for the intact rock I. When stress builds up to the point where a pre-existing plane t becomes unstable, shear failure occurs and fluid passes along the plane of the vein. The stress difference is reduced by the failure, and so the size of the Mohr circle shrinks, but the Mohr envelope is simultaneously displaced by fluid pressure change which causes an effective stress drop. If the stress state becomes asymmetric during the period of non-equilibrium loading, the Mohr circle may rise off the reference axis and touch the parabolic intact rock envelope at a single point with an angle of tangency different from the angle for the pre-existing plane of weakness. This may explain the development of a fringe of asymmetric, en échelon veins as after-shocks around the edge of an extant vein. In the absence of stress asymmetry, one would expect to see a pair of conjugate en échelon vein arrays of opposing sense.

STRAIN THEORY

Whilst deformation is known to be rotational in general, therefore requiring an asymmetric tensor representation, strain analysts have usually concentrated on the

practical goal of measuring the irrotational component of deformation, using methods such as R_f/ϕ analysis (Dunnet 1969) or the Fry technique (Fry 1979). The amount of rotation in a finite deformation is rarely quantifiable, except where a rigid block contains paleomagnetic indicators, but a sense of rotation can commonly be deduced. The vortical nature of flow has been recognized in mylonites and has been described using an asymmetric velocity gradients tensor (Truesdell 1954, Means *et al.* 1980, Lister & Williams 1983, Passchier 1986, 1987, 1988). It is now possible to measure the sense of vorticity (Simpson & Schmid 1983, Hanmer & Passchier 1991), the ratio of strain rate to recrystallization rate (Passchier & Simpson 1986) and the cumulative ratio of pure shear to simple shear in a general shear zone (Simpson & De Paor 1993), provided one assumes constant flow conditions. However, it is known that deformation events wax and wane with periods of accelerating and decelerating flow during which the instantaneous strain axes spin, yet acceleration gradients in rocks have not been addressed by structural geologists.

Rotational deformation and vortical flow

Figure 6 illustrates the Mohr construction for rotational deformation (De Paor 1983, De Paor & Means 1984), a polar plot in which stretch, S, is the radial co-ordinate and rotation, α, is the tangential co-ordinate. The distinction between this construction and that of Means (1983) merits some explanation. Because the co-ordinates are polar, the vertical is chosen as zero direction and so the circle is centered on a vertical axis when deformation is irrotational. Dextral rotation shifts the circle off-axis to the right and sinistral shifts it to the left. The Mohr circle's pole, P, is an anchor point (Simpson & De Paor 1993) through which lines drawn in particular spatial orientation (a, b, c) may be linked to corresponding points on the polar plot. Means's (1983) pole would plot diametrically opposite P. The open dots in Fig. 6(a) represent three arbitrary combinations of stretch and rotation (S, α) which plot on the perimeter of the Mohr circle. The second points of intersection with the Mohr circle, labelled Q_a, Q_b, Q_c are joined to the pole P to give the spatial orientations of dotted lines a, b and c in the final state. Angles are measured in the same sense in Mohr space and geographical space as indicated by the arrow. The initial orientation, PQ_0, of a line, and its rotation, α, to the final orientation, are obtained (Fig. 6b) by dropping a vertical line (dotted) from point S to point Q_0 on the Mohr circle and then joining Q_0 through P (dotted line). The sense of rotation, α, is correctly represented in Mohr space and geographic space, as indicated by the arrows.

Polar loci of stretch, shear strain and rotation

To determine the shear strain of any line with final orientation PQ in geographical space, the line's stretch S is located on the Mohr circle and the initially perpendicular stretch $S^{\perp}$ is marked diametrically opposite S

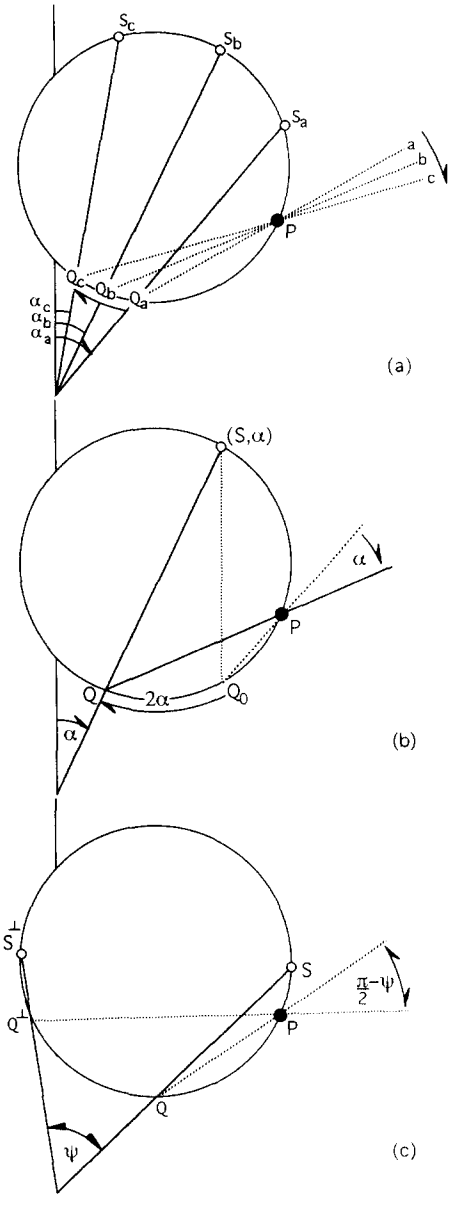

Fig. 6. (a) Polar Mohr construction for stretch S (radial co-ordinate) and rotation α (tangential co-ordinate). Open dots labeled S_a, S_b and S_c represent three lines a, b and c. Points labeled Q_a, Q_b and Q_c are second intersection points as explained in text. Arrows indicate compatible senses of angles measured in geographical and Mohr space. (b) Construction relating initial (dotted) and final (solid) line orientations after stretch, S, and rotation, α. Sense of rotation indicated by arrows. Angle α is doubled on the perimeter of the Mohr circle. See text for explanation. (c) Construction for angular shear ψ of dashed lines QP, $Q^{\perp}P$. Their stretches S, $S^{\perp}$ plot diametrically opposite each other on the Mohr circle.

(Fig. 6c). The second intersection point $Q^{\perp}$ is joined to the pole P to give the final orientation $PQ^{\perp}$ of a line initially perpendicular to PQ and the subtended angle, $\pi/2 - \psi$, gives the deflection from orthogonality. The required angular shear is ψ and the shear strain is $\gamma = \tan(\psi)$. Interesting patterns are obtained (Fig. 7) by plotting polar loci of stretch, S, and shear strain, γ, for (a) symmetric and (b) asymmetric deformation tensors. The distance along a ray from the origin to the strain ellipse (solid line) gives the stretch S for the ray's final orientation and the distance to the four-leaved locus (light line) gives the magnitude of the shear strain γ (the

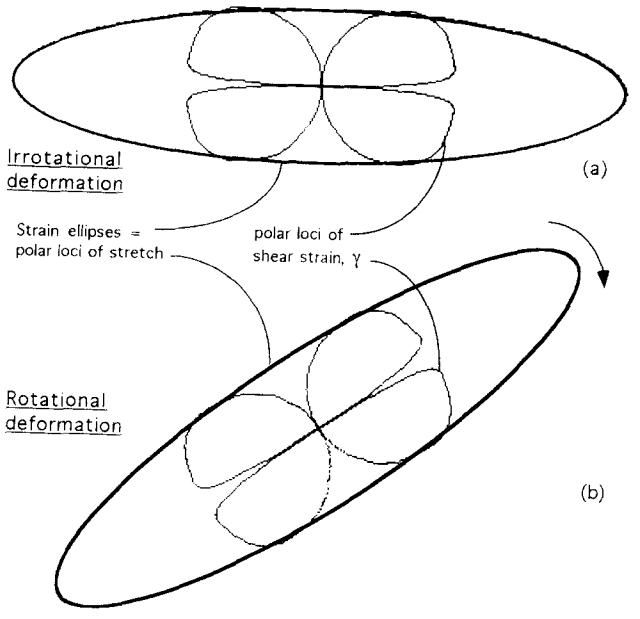

Fig. 7. (a) Loci of stretch S (bold ellipses) and shear strain γ (thin four-leaf curves) for symmetric deformation tensor. (b) Same loci retain their symmetry for asymmetric deformation. Arrow indicates sense of rotation of ellipse long axis.

same unit was chosen for unit stretch and unit shear strain). Note that the shear strain locus retains mirror symmetry with respect to the principal directions despite the asymmetry of the deformation tensor. This demonstrates the fundamental difference between shear strain and shear stress, which was found to be asymmetric for asymmetric stress states (Fig. 3b). The orthorhombic, rather than tetragonal, symmetry of the shear strain loci demonstrates that shear strains of finally orthogonal lines differ in magnitude, in contrast to shear strains of initially orthogonal lines.

Unlike loci of shear strain, loci of rotation (Figs. 8a–c) show a marked asymmetry in asymmetric deformation (cases b and c). This asymmetry comprises an obliquity to the principal directions and a skewness when compared with the symmetric case of Fig. 8(a). The distance along a ray represents the rotation in radians for a line in the final orientation of the ray (the same unit is used for radians and stretch). The locus for sub-simple shear (De Paor 1983) contains two directions of no rotation separating relatively large, dextral, forward rotations from relatively small, sinistral, back-rotations. The super-simple shear locus (Fig. 8c) has a skewed dumb-bell shape reflecting the rotation of all lines in a dextral sense but by differing amounts.

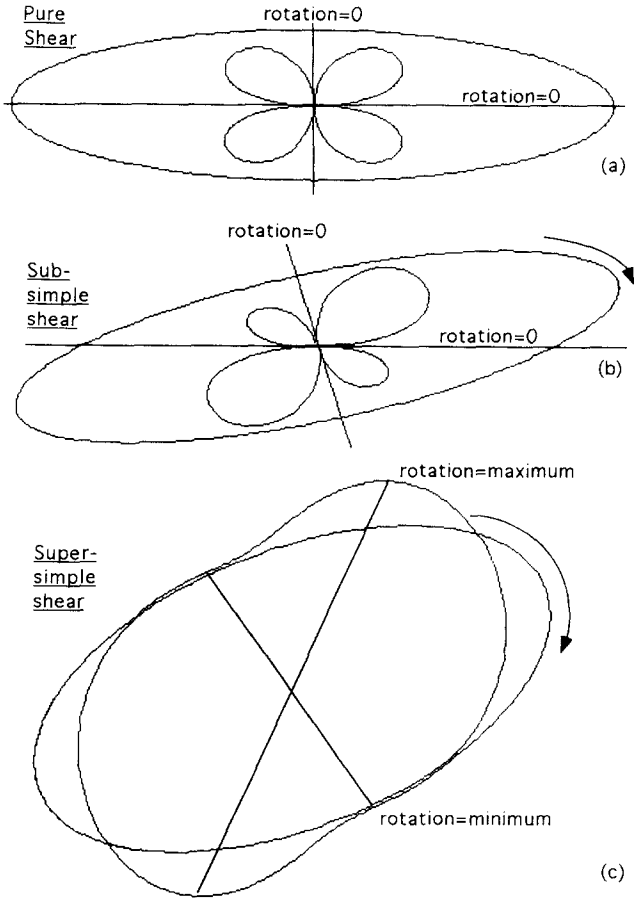

Fig. 8. Loci of stretch (ellipses) and rotation (other curves) for (a) pure shear, (b) sub-simple shear and (c) super-simple shear. Straight lines mark eigendirections (directions of no rotation) in (a) and (b). In (c), lines mark minimum and maximum rotation directions in the final state.

ACCELERATING FLOW

To describe accelerating deformation, we employ the Mohr constructions for flow and acceleration illustrated in Figs. 9(a) & (b), respectively. Two examples of unsteady flow are illustrated; in Fig. 9(c), deformation begins as pure shear but with time becomes increasingly dominated by simple shear whilst in Fig. 9(d), an initial increment of simple shear is followed by dominantly

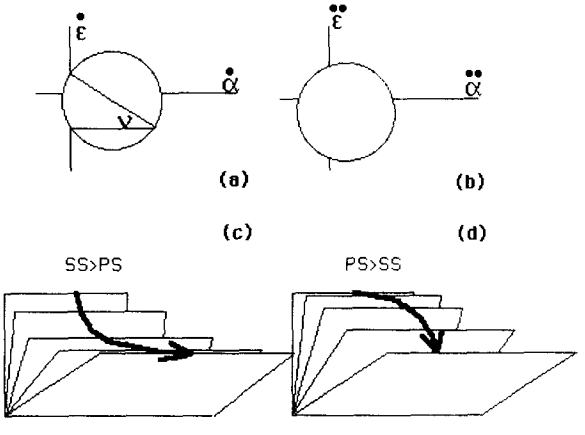

Fig. 9. (a) Off-axis Mohr construction for flow (velocity gradients tensor). Vertical axis represents longitudinal strain rate, horizontal axis represents rate of rotation of material lines. Vertical offset of Mohr circle related to Passchier's dilatancy number. Horizontal offset determined by vortical component of flow. Cos(ν) is the kinematic vorticity number (Bobyarchick 1986). (b) Off-axis Mohr construction for acceleration gradients. Vertical axis represents rate of stretching, horizontal axis represents angular acceleration of material lines. (c) Unsteady flow involving more simple shear with time. (d) Unsteady flow involving more pure shear with time.

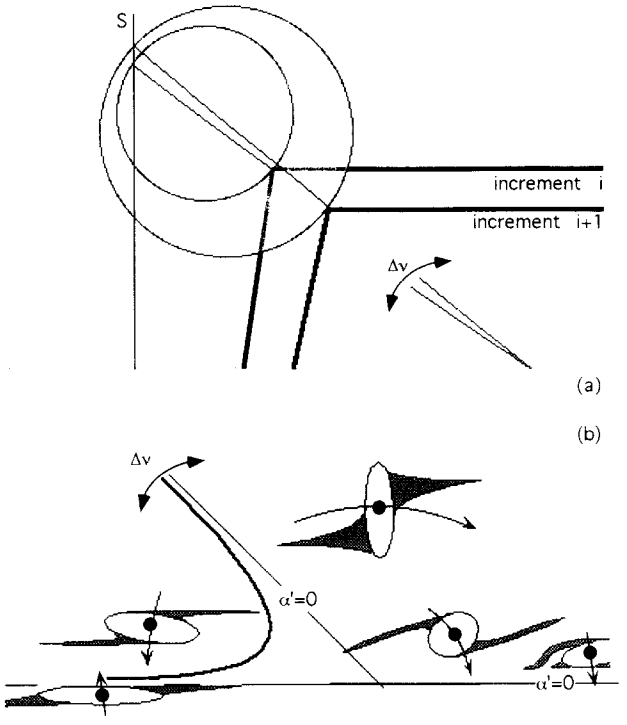

Fig. 10. (a) Close-up view of the top left-hand corner of deformed unit square and off-axis Mohr circles for two unsteady strain increments i and $i + 1$. Change $\Delta\nu$ in inclined ν eigenvector in region marked by double-headed arrow results in zone of rotation reversal. (b) Polar plot of axial ratio vs orientation of porphyroclasts showing sense of rotation and eigenvectors of flow regime (straight lines). Also shown are locus of end-orientations (bold hyperbolic curve) and zone subject to rotation reversal during spin of the flow field (double-headed arrow). Straight lines are eigendirections. Note paucity of fabric elements oriented in directions that might record rotation reversal.

pure shear. In both cases, there is a gradual change $\Delta\nu$ in the angle ν between lines of no angular velocity (flow eigenvectors or apophyses, $\alpha' = 0$) so that directions oriented between the inclined eigenvector for a deformation increment, i, and the next increment, $i + 1$, change their sense as well as their rate of rotation. However, the effects of acceleration on visible rock fabrics may not be great because the directions concerned may not be populated by many identifiable fabric elements. Figure 10 is a polar plot of object axial ratio vs orientation (see Simpson & De Paor 1993). The directions of dynamically recrystallized tail growth are all safely within the field of forward rotation and a slight change in the angle ν between the eigenvectors does not deflect them. The best opportunity for retaining a record of unsteady flow occurs when crystals grow during deformation. Elongate inclusions may then serve as longitudinal markers and they may reveal a gradual change in the angle between eigenvectors. Finally, it should be noted that sudden changes in flow regime are more likely to leave a recognizable signature in the form of fabric discontinuities. Indeed, many of the truncation structures described by Bell & Johnson (1989) and Bell *et al.* (1992) might be amenable to reinterpretation in terms of unsteady flow and pulsating porphyroblast growth. Future field and laboratory research should investigate this possibility.

CONCLUSIONS

Continuum mechanics has greatly aided our understanding of geological structures (Nadai 1950, Biot 1965, Ramsay 1967, Jaeger & Cook 1968, Ramberg 1975, Means 1976, Mandl 1988, Bayly 1992). However, many assumptions introduced by continuum mechanicists were intended to render theoretical systems simple enough to be described mathematically and need to be reviewed in practical rock deformation studies. With the aid of off-axis Mohr circles, stress may be viewed as an asymmetric tensor phenomenon, deformation as an impure, unsimple and inhomogeneous transformation, and flow as an unsteady phenomenon involving inflation or deflation and spinning acceleration. The result of such relaxation of assumptions is a loss of quantitative constraint; however, truly quantitative estimates of deformation conditions are extremely rare, difficult to evaluate for accuracy and precision, and of questionable intrinsic value (does it matter whether a stress is 5.0 or 5.1 MPa, whether a strain ratio is 2.5:1 or 2.6:1 or whether a kinematic vorticity number is 0.6 or 0.65?). A semi-qualitative descriptive system that approximates what is seen in rocks is preferable to a rigorously quantitative one that ignores reality. The merit of the approach taken in this paper should be judged in terms of the insight gained by students of structures in the field.

Acknowledgements—The author acknowledges support from NSF grant EAR-9219390. Thanks are due to Professor Charles Holland and Dr Dave Johnston for facilities provided at Trinity College, Dublin, during a short study visit. Helpful reviews by Cees Passchier and an anonymous referee are acknowledged. I particularly thank Win Means for help far beyond normal editorial duties.

REFERENCES

Allison, I. 1984. The pole of the Mohr diagram. *J. Struct. Geol.* **6**, 331–334.
Bayly, B. 1992. *Mechanics in Structural Geology*. Spring, New York.
Bell, T. H. & Johnson, S. E. 1989. Porphyroblast inclusion trails: the key to orogenesis. *J. metamorph. Geol.* **7**, 279–310.
Bell, T. H., Forde, A. & Hayward, N. 1992. Do smoothly curving spiral-shaped inclusion trails signify porphyroblast rotation? *Geology* **20**, 59–62.
Biot, M. A. 1965. *Mechanics of Incremental Deformation*. Wiley, New York.
Bobyarchick, A. R. 1986. The eigenvalues of steady state flow in Mohr space. *Tectonophysics* **122**, 35–51.
Cosserat, E. & Cosserat, F. 1909. See Truesdell & Toupin (1960).
De Paor, D. G. 1981. Geological strain analysis. Unpublished Ph.D. thesis, National University of Ireland.
De Paor, D. G. 1983. Orthographic analysis of geologic structures. I. Deformation theory. *J. Struct. Geol.* **5**, 255–278.
De Paor, D. G. 1987. Stretch in shear zones—implications for section balancing. *J. Struct. Geol.* **9**, 893–895.
De Paor, D. G. 1990. The theory of shear stress and shear strain on planes inclined to the principal directions. *J. Struct. Geol.* **12**, 923–927.
De Paor, D. G. & Means, W. D. 1984. Mohr circles of the first and second kind and their use to represent tensor operations. *J. Struct. Geol.* **6**, 693–701.
Dunnet, D. 1969. A technique of finite strain analysis using elliptical particles. *Tectonophysics* **7**, 117–136.
Engelder, T. & Geiser, P. 1980. On the use of regional joint sets as trajectories of paleostress fields during the development of the Appalachian Plateau, New York. *J. geophys. Res.* **85**, 6319–6341.

Fry, N. 1979. Random point distributions and strain measurement in rocks. *Tectonophysics* **60**, 89–105.
Günter, A. 1958. See Truesdell & Toupin (1960).
Hanmer, S. & Passchier, C. W. 1991. Shear sense indicators: a review. *Geol. Surv. Can. Pap.* **90–17**.
Huen, K. 1913. See Truesdell & Toupin (1960).
Jaeger, J. C. & Cook, N. G. W. 1968. *Fundamentals of Rock Mechanics*. Methuen, London.
Koenemann, F. H. 1992. Why is the stress tensor symmetric? (Abs.) Tectonic Studies Group, Geological Society of London Annual General Meeting, Southampton, U.K.
Kröner, K. 1887. See Truesdell & Toupin (1960).
Lister, G. S. & Williams, P. F. 1983. The partitioning of deformation in flowing rock masses. *Tectonophysics* **92**, 1–33.
Malvern, L. E. 1969. *Introduction to the Mechanics of a Continuous Medium*. Prentice-Hall, Englewood Cliffs, New Jersey.
Mandl, G. 1988. *Mechanics of Tectonic Faulting: Models and Basic Concepts*. Elsevier, Amsterdam.
Means, W. D. 1976. *Stress and Strain*. Springer, New York.
Means, W. D. 1982. An unfamiliar Mohr circle construction for finite strain. *Tectonophysics* **80**, T1–T6.
Means, W. D. 1983. Application of the Mohr-circle construction to problems of inhomogeneous deformation. *J. Struct. Geol.* **5**, 279–286.
Means, W. D., Hobbs, B. E., Lister, G. S. & Williams, P. F. 1980. Vorticity and non-coaxiality in progressive deformations. *J. Struct. Geol.* **2**, 371–378.
Nadai, A. 1950. *Theory of Flow and Fracture of Solids*. McGraw-Hill, New York.
Passchier, C. W. 1986. Flow in natural shear zones—the consequences of spinning flow regimes. *Earth Planet. Sci. Lett.* **77**, 70–80.
Passchier, C. W. 1987. Stable positions of rigid objects in non-coaxial flow—a study in vorticity analysis. *J. Struct. Geol.* **98**, 679–690.
Passchier, C. W. 1988. Analysis of deformation paths in shear zones. *Geol. Rdsch.* **77**, 308–318.
Passchier, C. W. & Simpson, C. 1986. Porphyroclast systems as kinematic indicators. *J. Struct. Geol.* **8**, 831–843.
Ramberg, H. 1975. Particle paths, displacement, and progressive strain applicable to rocks. *Tectonophysics* **28**, 1–37.
Ramsay, J. G. 1967. *Folding and Fracturing of Rocks*. McGraw-Hill, New York.
Ramsay, J. G. & Graham, R. H. 1970. Strain variations in shear belts. *Can. J. Earth Sci.* **7**, 786–813.
Simpson, C. & De Paor, D. G. 1993. Strain and kinematic analysis in general shear zones. *J. Struct. Geol.* **15**, 1–20.
Simpson, C. & Schmid, S. M. 1983. An evaluation of criteria to determine the sense of movement in sheared rocks. *Bull. geol. Soc. Am.* **94**, 1281–1288.
Truesdell, C. 1954. *The Kinematics of Vorticity*. *Indiana Univ. Sci. Ser.* **19**. University Press, Bloomington, Indiana.
Truesdell, C. & Toupin, R. A. 1960. The classical field theories. In: *Encyclopedia of Physics*, Volume 3 (edited by Flügge, S.), 226–793.
Voigt, W. 1887. See Truesdell & Toupin (1960).
Voigt, W. 1895. See Truesdell & Toupin (1960).